Journal Name

ARTICLE

Development of radiodetection systems towards miniaturised quality control of PET and SPECT radiopharmaceuticals†

matReceived 00th January 20xx,
Accepted 00th January 20xx

DOI: 10.1039/x0xx00000x

Matthew P. Taggart,[a] Mark D. Tarn,[b,c] Mohammad M. N. Esfahani,[d] Daniel M. Schofield,[e] Nathaniel J. Brown,[d] Stephen J. Archibald,[b,c] Tom Deakin,[a,e] Nicole Pamme[c,§] and Lee F. Thompson[a,‡]

The ability to detect radiation in microfluidic devices is important for the on-chip analysis of radiopharmaceuticals, but previously reported systems have largely suffered from various limitations including cost, complexity of fabrication, and insufficient sensitivity and/or speed. Here, we present the use of sensitive, low cost, small-sized, commercially available silicon photomultipliers (SiPMs) for the detection of radioactivity inside microfluidic channels fabricated from a range of conventional microfluidic chip substrates. We demonstrate the effects of chip material and thickness on the detection of the positron-emitting isotope, [^{18}F]fluoride, and found that, while the SiPMs are light sensors, they are able to detect radiation even through opaque chip materials via direct positron and gamma (γ) ray interaction. Finally, we employed the SiPM platform for analysis of the PET (positron emission tomography) radiotracers 2-[^{18}F]fluoro-2-deoxy-D-glucose ([^{18}F]FDG) and [^{68}Ga]gallium-citrate, and highlight the ability to detect the γ ray emitting SPECT (single photon emission computed tomography) radiotracer, [^{99m}Tc]pertechnetate.

Introduction

The field of nuclear medicine includes two very important medical imaging techniques for diagnosis and monitoring in oncology, cardiology and neurology: positron emission tomography (PET) and single photon emission computed tomography (SPECT).[1] Both rely on the injection of a radioisotope-labelled compound, a so-called radiotracer or radiopharmaceutical, into the patient that targets specific conditions or diseases and allows their position to be located via radiodetectors. PET employs radiotracers labelled with positron (β^+)-emitting isotopes (e.g. ^{18}F, ^{11}C, ^{68}Ga, ^{64}Cu), which release positrons that annihilate with electrons to form two anti-parallel gamma (γ) rays (511 keV each) that are picked up by a ring of radiodetectors.[1-3] SPECT typically utilises radioisotopes that directly emit γ rays (e.g. ^{99m}Tc, ^{123}I, ^{67}Ga) and picks up the signals using a gamma camera.[1, 4, 5]

PET in particular has recently begun to experience a paradigm shift in terms of the production of radiotracers. Conventionally, such tracers are generated in large batches in a production facility before being transported to the imaging centre, and are often restricted to the most widely used PET radiotracer: 2-[^{18}F]fluoro-2-deoxy-D-glucose ([^{18}F]FDG).[6-8] While this is cost effective, it results in a "one-size-fits-all" scenario that is not necessarily optimal for the patient. In recent years the concepts of "decentralised production" [9-11] and "dose-on-demand" [12-15] have gained a great deal of interest, whereby a single dose of the most suitable radiotracer would be produced on-site for a specific patient or group of patients, enabling a more stratified approach to patient treatment.

Key to dose-on-demand is the use of microfluidic devices,[16] which are ideally placed to handle and synthesise the low volumes of radioactive solutions available, whilst reducing shielding requirements and radiation exposure to personnel. Indeed, the synthesis of PET radiotracers, particularly [^{18}F]FDG, in microreactors has been under development for a decade,[10, 11, 17-23] but it is only recently that such devices have reached sufficient maturity for release onto the market. However, while the radiosynthesis step has been successfully miniaturised, other aspects of radiotracer production have largely been ignored, including the quality control (QC) testing steps that are essential in ensuring the safety and purity of the radiotracer dose. For example, [^{18}F]FDG requires a number of QC tests,[24, 25] many of which require some form of radiation detection for determination of: activity (in units of becquerel, Bq, or curie, Ci), half-life ($t_{½}$, for identification/confirmation of

[a] Department of Physics and Astronomy, University of Sheffield, Hounsfield Road, Sheffield, S3 7RH, UK. E-mail: l.thompson@sheffield.ac.uk; Tel: +44 (0) 114 2224577; Fax: +44 (0) 114 2223555.
[b] Positron Emission Tomography Research Centre, University of Hull, Cottingham Road, Hull, HU6 7RX, UK.
[c] Department of Chemistry, University of Hull, Cottingham Road, Hull, HU6 7RX, UK. E-mail: n.pamme@hull.ac.uk; Tel: +44 (0) 1482 465027; Fax: +44 (0) 466410.
[d] School of Engineering, University of Hull, Cottingham Road, Hull, HU6 7RX, UK.
[e] LabLogic Systems Ltd., Paradigm House, 3 Melbourne Avenue, Broomhill, Sheffield, S10 2QJ, UK.
‡ Corresponding author for radiodetection.
§ Corresponding author for microfluidics.
† Electronic Supplementary Information (ESI) available: Additional experimental detail and results obtained using a PTFE microfluidic chip substrate. See DOI: 10.1039/x0xx00000x

the radionuclide, e.g. ^{18}F), and radiochemical purity/identity via thin layer chromatography with a radiodetector (radio-TLC) and high performance liquid chromatography with a radiodetector (radio-HPLC).

We are developing an integrated microfluidic platform for the quality control testing of PET radiopharmaceuticals,[26, 27] and a crucial aspect of such a platform is the incorporation of suitable miniaturised radiodetectors. Only a handful of such detectors have thus far been demonstrated with microfluidic systems, often via the detection of Cherenkov light,[28] emitted when a charged particle travels through a medium (with refractive index, *n*) at a velocity (*v*) faster than the phase velocity of light through that medium (i.e. $v > c/n$), or scintillation light;[29] photons generated by electrons that have been excited by ionising radiation falling back to lower atomic levels. Examples of on-chip radiodetection include performing conventional autoradiography via phosphor imaging of chips[30-32] imaging via plastic scintillators[33] and inorganic scintillators,[34, 35] Cherenkov imaging via a CCD camera,[36-38] a PIN silicon photodiode array,[39-41] a solid-state beta-particle camera consisting of a position-sensitive avalanche photodiode (PSAPD),[42-45] and the use of liquid scintillators within microfluidic channels.[46, 47] However, these methods can suffer from limitations including expense, size, speed, sensitivity, and complexity of fabrication.

Here, we investigate the potential of silicon photomultiplier (SiPM) technology for radiation detection, with a view to future incorporation into an integrated QC platform. SiPMs are solid-state silicon-based photodiode light detectors[48, 49] that are sensitive to single photons, with a dark count rate of <100 kHz mm^{-2}, and have recently improved greatly in terms of price and sensor size, as well as in performance which is approaching that of conventional PMTs. SiPMs have become especially suited to scaled-down systems, making them ideal for integration with microfluidic systems. Here, we evaluate the performance of an array of SiPMs for the detection of radiation from the positron-emitting isotope, [^{18}F]fluoride, in a microfluidic channel, with an initial view to determination of the activity and half-life of synthesised radiotracers. We further study the effect of commonly used microfluidic substrates and substrate thickness on the detection signal, and study the origins of the detection signal. Finally, we apply the SiPM platform to the on-chip analysis of the clinically relevant PET radiotracers, [^{18}F]FDG and [^{68}Ga]gallium-citrate, and the SPECT radiotracer, [^{99m}Tc]pertechnetate.

Experimental

Chemicals and reagents

All solutions and dilutions were prepared in high purity water (18.2 MΩ cm at 25 °C) that had been double-filtered (0.05 μm) through an ELGA Option 4 system that fed into an ELGA UHG PS system (ELGA Process Water, Marlow, UK). Hydrochloric acid (37 %) for elution of [^{68}Ga]gallium from a generator was purchased from Fisher Scientific (Loughborough, UK). A solution of 0.1 M citric acid was prepared for [^{68}Ga]gallium labelling by dissolving 0.42 g of the citric acid (Fisher Scientific) in 20 mL of water.

All chemicals for [^{18}F]fluoride production and [^{18}F]FDG synthesis were purchased from ABT Molecular Imaging (Knoxville, TN, USA) and used without further purification. Original suppliers of these chemicals were Rotem Industries Ltd. (Israel) for the ^{18}O-enriched (>95 %) target water, and ABX GmbH (Radeberg, Germany) who supplied the vials of mannose triflate, phase transfer catalyst (containing cryptand 2.2.2 and potassium carbonate in acetonitrile with a small amount of water), acetonitrile, water for injection, and hydrochloric acid (2 M).

Preparation of radioisotopes and radiotracers

[^{18}F]fluoride radioisotope

[^{18}F]fluoride radioisotope was prepared by proton bombardment of 280 μL of ^{18}O-enriched target water, via the ^{18}O(p,n)^{18}F nuclear reaction, using the BG75 Biomarker Generator cyclotron (ABT Molecular Imaging).[15, 50] Irradiation of the target water was performed with a 7.5 MeV proton beam (4.2 μA). The [^{18}F]fluoride was then transferred automatically to a 1.5 mL Eppendorf tube for further

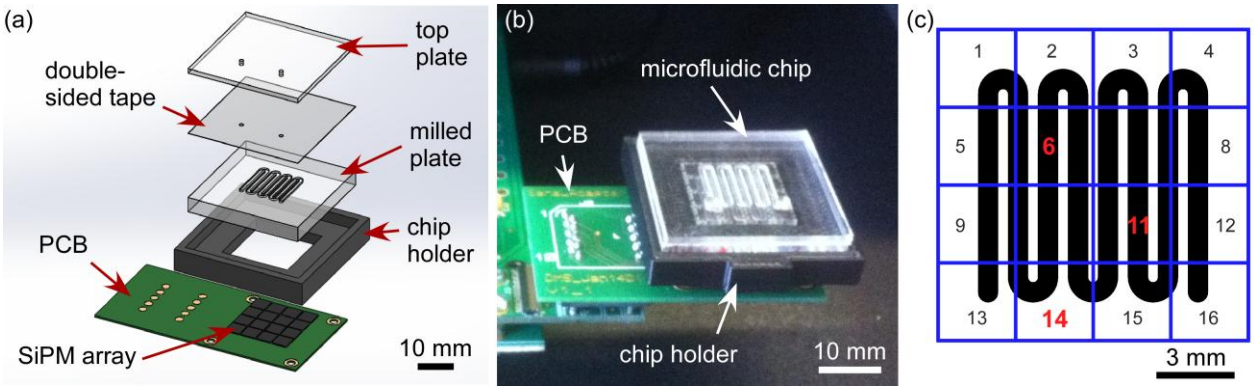

Fig. 1 Setup of the microfluidic chip and silicon photomultiplier (SiPM array). (a) Exploded schematic of the microfluidic chip, consisting of a milled serpentine channel in a substrate that was bonded to a top plate. The milled plate material and thickness was varied throughout this work. The completed chip was situated in a chip holder over a silicon photomultiplier (SiPM) array. (b) Photograph of the final chip setup on the SiPM array. (c) Schematic depicting the relative position of the microfluidic channel to the SiPM cells. Cells 6, 11, and 14 (highlighted in red) were used for counting of activity in the microchannel.

processing. Dilutions were prepared as necessary with purified water in order to achieve the desired activity per volume (i.e. MBq mL^{-1}).

[^{18}F]FDG radiotracer

[^{18}F]FDG radiotracer was prepared by first generating the [^{18}F]fluoride ion as described above. However, following proton bombardment the radioisotope was instead transferred to the BG75 Biomarker Generator's Card Chemistry System (CCS),[15, 50] which had been pre-prepared with reagent vials. [^{18}F]FDG synthesis was performed using a dose synthesis card (DSC), which allows production on a dose-on-demand basis via nucleophilic substitution of mannose triflate with [^{18}F]fluoride.[6] A sample of [^{18}F]FDG was automatically injected into the BG75's automated quality control platform to test for chemical and radiochemical purity,[15, 50, 51] while the remainder of the dose (~2.3 mL) was dispensed into a syringe for collection.

[^{68}Ga]gallium-citrate radiotracer

[^{68}Ga]gallium was eluted from a 740 MBq ^{68}Ga/^{68}Ge generator (iThemba LABS/IDB Holland) in 0.6 M HCl and processed for synthesis as described in the literature.[52] Briefly, the eluate was purified via retention on a Strata-X-C strong cation exchange column (Phenomenex, Macclesfield, UK), before being eluted in a mixture (98:2) of acetone and 0.1 M hydrochloric acid. The purified [^{68}Ga]gallium was then dried under vacuum at 90 °C in a heating block. Once cooled to room temperature, a 0.1 M solution of citric acid was added to the dried [^{68}Ga]gallium and allowed to react for 15 min with agitation to form a solution of [^{68}Ga]gallium-citrate radiotracer.

[^{99m}Tc]pertechnetate radiotracer

A solution of the gamma-emitting radioisotope, [^{99m}Tc]technetium, was eluted from an 2.15 GBq Ultra-Technekow DTE ^{99}Mo/^{99m}Tc generator (Mallinkrodt Pharmaceuticals, Ireland) in saline solution as sodium [^{99m}Tc]pertechnetate ($Na^{99m}TcO_4$). This was used without further processing other than dilution in purified water to the desired activity.

SiPM detector design

The detection setup consisted of a SensL C-Series MicroFC-SMA-30035 4x4 SiPM array (SensL, Cork, Ireland) (Fig. 1). The 30035 model contains 4774 microcells per 3 x 3 mm^2 cell, allowing for a significant dynamic range, and the 4 x 4 SiPM array thus consisted of sixteen of these cells packed such that there was only 200 μm of inactive space between adjacent cells. The system read-out was via SensL's own evaluation/preamplifier board sections (model numbers: ArraySB4-EVB-PixOut, ArraySB4-EVB-PreAmp) with an adaptor break-out board courtesy of LabLogic Systems Ltd. (Sheffield, UK) for use with the C-Series SiPM array. This allowed full access to the individual and summed outputs of the device. The preamplifier board provided the 5 V power supply required, while the bias voltage of 28 V was supplied via an external power supply unit (Aim and Thurlby Thandar Instruments, Cambridgeshire, UK). Fig. S1 in the ESI shows the disassembled components of the SiPM platform, and the complete setup.

Microfluidic chip design and fabrication

The microfluidic chip design consisted of a serpentine channel that was directly milled into square (30 mm x 30 mm) glass and plastic substrates via CNC micromachining[53] using a Datron M7 milling machine (Datron, Germany). The channel, which was designed to be filled with a known volume of solution while covering the entire area of the SiPM array (in particular the SiPM cells of interest), had a width of 1.0 mm, a depth of 450 μm, and a length of 94.2 mm, thereby holding an approximate volume of 40 ± 2 μL given tolerances of the manufacturing process (Fig. 1). Due to the fabrication technique, the channels featured an approximately square-section profile. All chips were sealed using a square (30 mm x 30 mm) top plate fabricated from 1.5 mm thick poly(methyl methacrylate) (PMMA) that was bonded with transparent double-sided tape (RS Components, Corby, UK) to the milled substrate. The top plate had an inlet hole and an outlet hole drilled into it (2 mm diameter each), while corresponding holes were punched into the double-sided tape prior to bonding.

Two main studies were performed using the devices to determine the effect of (1) the type of substrate material, and (2) the thickness of the substrate material. In the first scenario, the serpentine channel was fabricated in 4 mm thick substrates of poly(methyl methacrylate) (PMMA), polycarbonate (PC), B-270 crown glass, soda-lime glass, and Borofloat glass. The effect of substrate thickness was studied by milling the serpentine channel into polycarbonate substrates of 2 mm, 4 mm, 6 mm, 8 mm, 10 mm and 12 mm thickness.

The ability to detect radioactivity through opaque materials using the light-sensing SiPM array was tested by milling the channel into 4 mm and 8 mm thick PC substrates that were subsequently coated with aerosol gloss black spray paint (RS Components, Northants, UK), referred to as "PC opaque". Further tests were also performed using opaque chips fabricated from polytetrafluoroethylene (PTFE), with thicknesses of 2 mm and 12 mm.

Chip holders were produced to achieve consistent results by ensuring the location of the microfluidic channel with respect to the SiPM array, as depicted in Fig. 1. The holders were 3D-printed from opaque PLA (polylactic acid) using a Makerbot Replicator 2X 3D printer. Their dimensions were 35 mm long x 35 mm wide x 6 mm deep, and featured a 31 mm x 31 mm shelf on which to house the chip. An 18 mm x 18 mm window allowed the serpentine channel to be placed directly over the SiPM array. Thus, fixing the relative positions of the SiPM cells to the microfluidic channel ensured that the measured count rate was not artificially increased or decreased by varying the distance between the source and the detector.

Experimental procedure

Briefly, experiments were performed by filling the microfluidic channel with radioactivity, determining the amount of activity in the channel via a dose calibrator, and then placing the chip on the SiPM array for detection.

First, the required radioisotope/radiotracer was prepared and diluted with purified water such that 40 μL of solution would contain a desired level of radioactivity (in MBq) and thus concentration of radioactivity (i.e. MBq mL^{-1}) appropriate for each experiment. This 40 μL volume was introduced into one of the chip access holes via a pipette, after which a layer of tape was placed over the access holes to ensure that no evaporation could occur and to prevent contamination by spillage. The chip was then placed into the 3D printed chip holder, before measurement in a CRC-55t PET dose calibrator to determine the amount of activity at a reference time point, where after the level of activity remaining in the chip at certain time points could be determined using the half-life equation for the appropriate radiotracer.

With the known activity recorded, the chip (with holder) was then placed onto the SiPM array for data collection. The SiPM array was housed in a box with a fold-down lid to ensure that no external light could reach the detector. Data was recorded by monitoring detection signals from four of the SiPM outputs (Fig. 1c): two near the centre of the chip (outputs from cells 6 and 11), one near the inlet port (output from cell 14), and finally the summed output of all of the cells. Counting data from the radioactive sources was collected for 5 min by connecting the selected outputs to a CAEN N841 discriminator and CAEN N1145 quad scaler system. The discriminator threshold was set to 85 mV and 30 mV for the sum and individual outputs, respectively. These thresholds were selected by viewing pulses on a LeCroy Waverunner 6100 oscilloscope and triggering on the positive edge. ROOT software,[54] an open-source analysis framework, was used for analysis and plotting of collected counting data from output channel 11. Error bars are present for each data point in the plots throughout this paper, but it should be noted that in some cases the error bars are smaller than the size of the marker point.

Geant4 penetrability simulations

An initial study of SiPM performance had taken place prior to the work reported here, utilising a similar SiPM detector setup as described here but using a standard ^{22}Na disk source (Fig. S2 in the ESI) as a positron emitter (546 keV positron energy) to provide the subsequent 511 keV annihilation γ rays. To test the viability of detecting Cherenkov light using the SiPMs, which would directly examine the positron as opposed to the resultant γ rays, a series of Geant4 penetrability simulations were performed.[55] These investigated the maximum penetration depth of positron tracks from various potential positron emitters for several common microfluidic substrates. The results of these simulations are shown in Fig. 2, and confirm that while a ^{22}Na source is a suitable proxy as a source of annihilation photons (γ rays), the 546 keV positron itself would almost certainly be stopped within the plastic surround (~4 mm thick) of the ^{22}Na disk. This information allowed the prospective substrate thicknesses to be limited for subsequent studies.

Results and discussion

Effect of material type

Microfluidic chips were constructed from a variety of substrate materials consisting of a selection of plastics and glasses commonly used in microfluidics. The purpose here was to establish whether the SiPM response was a function of material choice. The glass chips tested were fabricated from B270 crown glass, Borofloat glass, and soda-lime glass, while the plastics consisted of polycarbonate (PC) and polymethyl methacrylate (PMMA). All of the milled substrates featuring the serpentine channel were 4 mm thick with a 1.5 mm thick PMMA top plate. Some of the physical properties of the

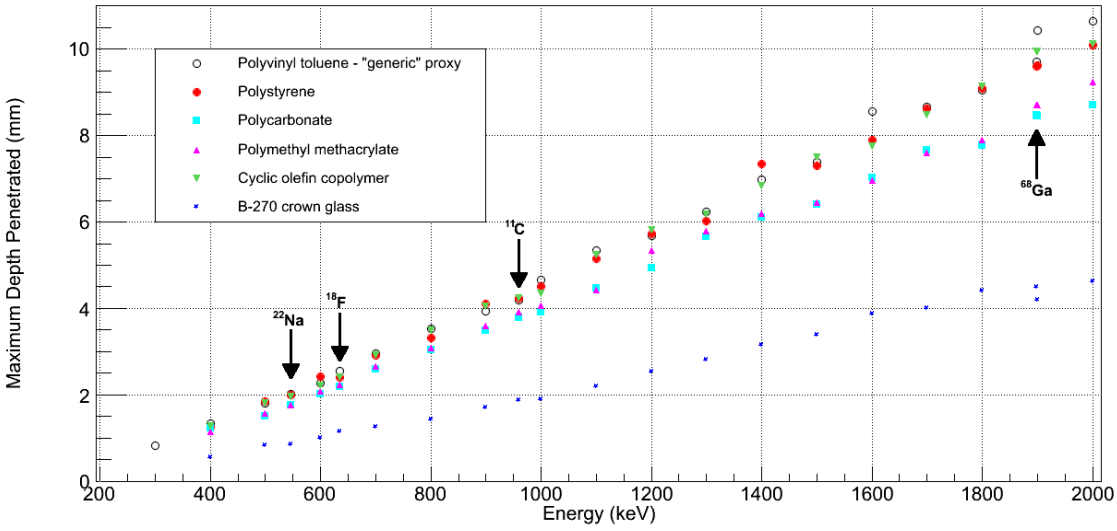

Fig. 2 Maximum depth of penetration for positrons in a variety of commonly used microfluidic substrate materials. The endpoint energies of positron-emitting isotopes of choice have been marked on the graph for reference.

materials are listed in Table S1 in the ESI. These properties directly affect positron penetrability, with the maximum depth of positron penetration expected to be lower for more dense materials.

A solution of [^{18}F]fluoride (40 μL) was added to each chip, the radioactivity level (in MBq) was then measured in a dose calibrator and the reference time recorded, before being placed on the SiPM array. The count rate observed by the SiPM was recorded over 5 minutes, and the resultant plot of SiPM count rate (counts per second, cps) versus radioactivity (MBq) is shown in Fig. 3a. High levels of radioactivity (e.g. 8 MBq) could yield ~10^5 counts over the 5 min time frame, giving count rates of around 300 cps. Comparatively, when the chips were placed on the SiPM array without any radioactivity as negative control tests, only 0 – 7 counts were recorded over 5 min, giving maximum count rates of 0.02 cps.

Results largely showed reasonable linearity for each material other than PMMA, and similar count rates were recorded. Unfortunately, a problem with the CNC milling of the PMMA chip caused its channel to be deeper than intended. This meant that the dose did not evenly distribute throughout the channel and some internal movement throughout the experiment is suspected. As a result, the plot points for PMMA show a great deal of variation around the best fit line, and while they show the general trend of decreasing count rate with decreasing activity, the results cannot be taken as absolute values for that material.

Discounting the PMMA material due to the aforementioned issues, the glass chips all exhibited lower count rates compared to the polymer PC chip, likely due to the higher density of the glasses (see Table S1 in the ESI) that would attenuate positrons/gamma rays to a greater extent than less dense plastics. However, given the densities of the materials, it may have been expected that Borofloat glass (ρ = 2.20 g cm^{-3}) would give the best results of the three glasses, followed by soda-lime (ρ = 2.52 g cm^{-3}) and then B270 (ρ = 2.55 g cm^{-3}), while in fact the opposite was observed, although the densities between the materials were largely quite similar. This may mean that at the 4 mm material thickness, the density of the material may not cause a huge effect on the detected signal and may be the result of other aspects such as material composition. Low-level fluorescence caused by exposure to radiation (i.e. scintillation) could be another potential source of signal in some of the materials, although none of the materials used here are known to have significant scintillating properties. Furthermore, due to the lack of a dopant present in the material, any such scintillation light would not necessarily be at a wavelength within the detector's spectral response range. These aspects will require further investigation in the future. Still, in all, these initial results demonstrated the suitability of the SiPM array for the detection of radiation from positron-emitting radioisotopes in a range of conventional microfluidic chip materials and with good linearity over a clinically relevant range.

Effect of material thickness

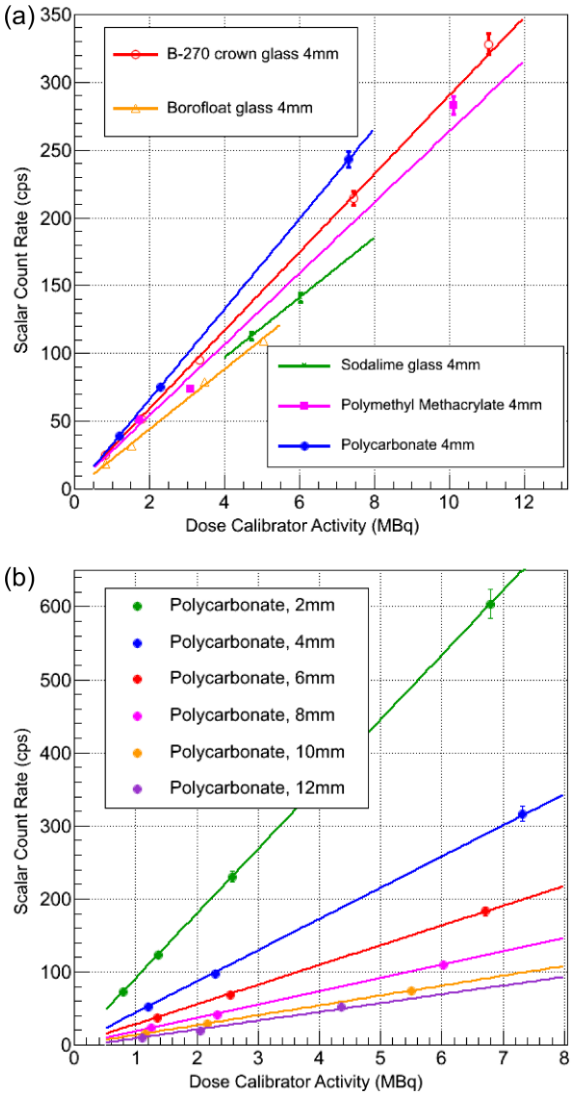

Fig. 3 Activity of the [^{18}F]fluoride ion in the microfluidic channel plotted against the SiPM signal count rate in (a) various substrate materials (4 mm thick), and (b) polycarbonate substrates of varying thickness. Only statistical uncertainties are displayed.

Having tested a range of chip materials, the next step was to determine the effect of the substrate thickness on the acquired signals by varying the distance between the SiPM array and radioisotope source in the microchannel. Polycarbonate was selected as the substrate for this investigation due to the ease with which to prepare the different thickness, ranging from 2 mm to 12 mm (with 2 mm intervals). As before, [^{18}F]fluoride was added to the chips and the count rates determined on the SiPM array for each chip, as shown in Fig. 3b.

All results showed good linearity of signal count rate with activity, with all data points lying within the error of the fit, and demonstrated that as the substrate thickness increased, the SiPM signal decreased. For the thinnest substrate tested (2 mm), the distance between the bottom of the microfluidic channel and the chip-SiPM interface was less than the

maximum penetrability of the ^{18}F positron (see Fig. 2), and so in this instance the positron could impinge on the SiPM surface. This can be observed in Fig. 3b where the 2 mm thick PC count rate is significantly higher than the spread of the 4-12 mm thick substrates, which indicates that the SiPMs are susceptible to direct positron interaction. By replotting Fig. 3b, the dependence of the SiPM signal intensity on the chip thickness can be further demonstrated for different activity levels (calculated based on the line equations obtained from Fig. 3b), and this is shown in Fig. S3 in the ESI. While it would be expected that thicker substrates would allow the generation of more Cherenkov light due to positrons being allowed to travel to their greatest extent and generate more light, the fact that the SiPM signal decreased with increasing thickness suggests that the Cherenkov component of the signal may in fact be minimal. Instead, a major source of the SiPM signal appears to be due to direct interaction with positrons, which clearly lessens as the substrate thickness increases. Some of the signal may also have been due to direct γ ray interaction with the SiPM array. Interestingly, Cho et al.[36] demonstrated previously that conventional photomultiplier tubes (PMTs) were also susceptible to direct interaction with the 511 keV γ rays resulting from positron-electron annihilation at high activity levels, yielding a signal even in the absence of light. Future work on this could involve a more focussed study on the contribution of each signal source (positron interaction, γ ray interaction, Cherenkov light, and possible scintillation) at different distances from the detector in order to better understand the relevant mechanisms and dependences, and to validate the theories and interpretation we have proposed here.

Material opacity study

In order to isolate the source of the pulses detected by the SiPM, a study was performed to remove the Cherenkov and potential scintillation components of the signal by comparing opaque substrate materials to transparent ones. Transparent PC chips were used just as before, while to prepare opaque chips the underside of 4 mm and 8 mm thick PC substrates were painted black, with an additional sheet of black plastic placed between the chip and the SiPM array (Fig. S3 in the ESI). The black plastic had been shown to completely attenuate the light from a blue LED placed in close proximity to the SiPM. The results for both the opaque and transparent 4 mm and 8 mm thick PC substrates are shown in Fig. 4, and demonstrate very similar effects between the opaque and transparent variations. The use of 4 mm, and particularly 8 mm, thick substrates meant that the SiPM array would have been shielded from direct positron interaction, while the use of paint and a plastic sheet shielded the SiPMs from Cherenkov emission and the possibility of scintillation light. Hence, the fact that signal could still be detected can only be explained if the SensL C-Series device is sensitive to low-energy γ rays created through the annihilation of the positron and any subsequent Compton scattering. The results showed that the transparent PC materials yielded slightly higher count rates than their opaque counterparts, likely due to the presence of Cherenkov light generated as positrons passed through the material, with low-level scintillation also a possibility. However, the relatively small differences between the opaque and transparent chip results suggested that the main components of the signal were due to direct positron and/or γ interaction with the SiPM.

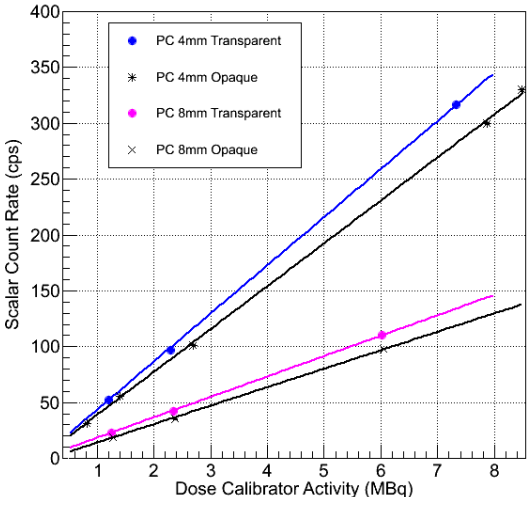

Fig. 4 Comparison of SiPM signal for transparent and opaque polycarbonate (PC) substrates. Signal was obtained even from the opaque materials.

Further tests were performed in which [^{18}F]fluoride was introduced into 2 mm and 12 mm thick substrates of opaque PTFE polymer. Signals were again detected even with the opaque materials, reiterating the conclusions of the previous opacity test (Fig. S4 in the ESI), while also demonstrating once more that the thinner substrate yielded much higher signals than the thicker substrate.

Linearity of [^{18}F]fluoride signal

Typical activities injected into a patient for a PET scan will be in the order of 370 MBq (10 mCi), while the actual volume of solution can vary (e.g. around 0.5-15 mL). The ABT Biomarker Generator produces [^{18}F]FDG in a dose-on-demand format, delivering a final syringe of 2.3 mL volume. Thus, if we assume a minimum activity of 370 MBq in that injection volume, as an example, then the "concentration" of activity would be 160 MBq mL^{-1}, or 0.16 MBq μL^{-1}. Thus, a minimum clinically relevant level of radioactivity from the ABT platform for detection with our system would be 6.4 MBq in the 40 μL channel volume. On the other hand, if 10 mL is taken as a typical or average injection volume, then the concentration would be 0.037 MBq μL^{-1} (37 MBq mL^{-1}) and so the activity in 40 μL would be 1.5 MBq. Furthermore, since 370 MBq would be used for an actual injection, any analysis taking place prior to injection would contain greater levels of activity than this.

In order to confirm that we were able to measure such clinically relevant activities, a new set of measurements was performed to test the linearity of the detection signal across this region of interest. [^{18}F]fluoride was introduced into 4 mm thick substrates of B-270 glass, PMMA, polycarbonate, and opaque polycarbonate (painted black and with a plastic sheet

placed between it and the SiPM array, as described earlier). The major difference between this study and the earlier material investigation was the range of activities that were tested, with activities measured between ~100 MBq and ~0.01 MBq in the microfluidic chip at several time points. The results of this extended linearity study are shown in Fig. 5a. Uncertainties in the data points comprised the √*n* statistical component as well as a 10 % systematic error. This allowed coverage across four orders of magnitude in activity, and confirmed the linearity of our system across the clinically relevant region, highlighting the suitability of the technique for the analysis of PET radiotracers. With this, it should be feasible, upon preparation of a calibration curve of SiPM signal versus activity for a given microfluidic chip (standardised material, thickness and channel design etc.) and a given radioisotope-labelled pharmaceutical, to determine the level of radioactivity in an unknown sample, akin to a dose calibrator, as part of an integrated platform in which the operator would not be required to directly handle any radioactivity. These results also demonstrate that while the current volume of solution in the microchannels (40 μL) is actually quite large from a microfluidics point-of-view, it could significantly reduced whilst still allowing detection in the relevant MBq range.

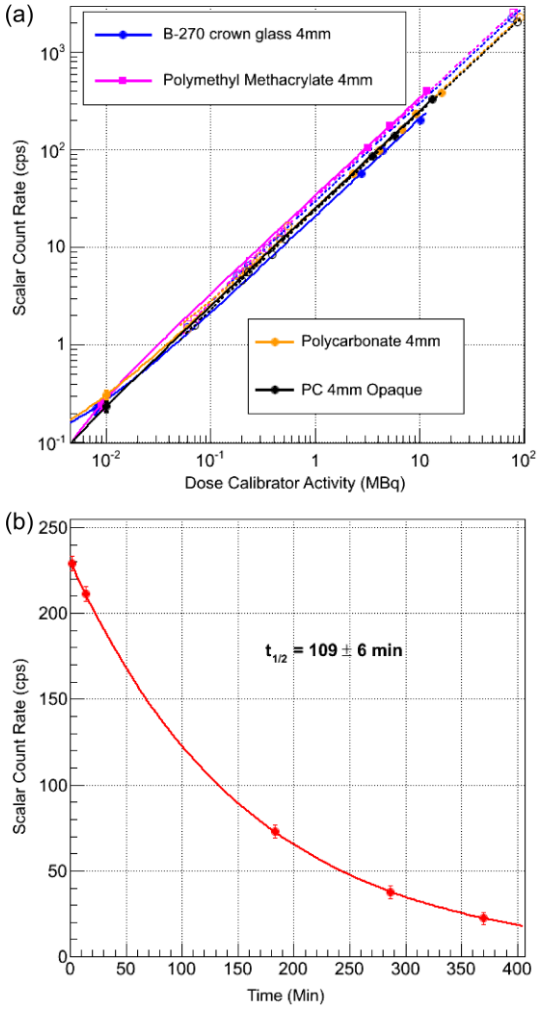

Fig. 5 (a) Study of the linearity of the SiPM signal over four orders of magnitude of [^{18}F]fluoride activity in 4 mm thick substrates. The uncertainties comprise the √*n* statistical component as well as a 10 % systematic error. (b) Determination of [^{18}F]fluoride half-life based on multiple measurements taken over several half-lives.

Half-life measurement of [^{18}F]fluoride

The determination, and confirmation, of the isotopic half-life ($t_{½}$) is a key QC criterion that must be met by any system intended to satisfy the "radionuclidic identity" test, to ensure that the radiation is due to the expected radioisotope source. [^{18}F]fluoride has a documented $t_{½}$ of 109.7 min.[56] According to the *British Pharmacopoeia 2012*, the approximate half-life of a [^{18}F]fluoride-labelled molecule should be determined "*by no fewer than 3 measurements of the activity of a sample in the same geometrical conditions within a suitable period of time (for example, 30 min)*", and results should yield a half-life between 105 to 115 min.[57] Some authors have suggested that a suitable time period is 20-30 min,[25] while others have suggested that as little as 10 min is suitable.[24, 58] Although no instrument is specified for the analysis, a dose calibrator is often employed.

In order to determine whether half-life could be calculated using the SiPM system, [^{18}F]fluoride was added to a polycarbonate chip (4 mm thick), the activity measured in a dose calibrator, and counting data taken for 5 min. The activity was allowed to decay over 6 hours, i.e. approximately three half-lives, and counting data taken at several points during this acquisition window. The results are shown in Fig. 5b, and from these the half-life was calculated to be 109 ± 6 min for [^{18}F]fluoride. This demonstrates the ability to obtain a fairly accurate value for the half-life of a radioisotope using the SiPM platform, although there are clearly some issues with precision (± 6 min) that would need to be addressed before use in a clinical setting could be achieved. Sources of noise and errors within the platform will need to be characterised in future tests. For example, such sources could include noise produced by the 20-to-40 pin adaptor situated between the SiPM array and the preamplifier board; a component that could be removed in a future iteration of the platform. Additional improvements to the precision could come from an optimised chip with a dedicated design, and further integration of the SiPM array (or a single SiPM) with the chip. Furthermore, while the 6 hour time frame is clearly unsuitable for a miniaturised QC package, it nonetheless indicates that the system is capable of making accurate half-life measurements, albeit with a need for further optimisation.

In addition to the 5 min counts that were taken during the previous analysis of half-life, a series of shorter time base measurements were also taken in order to ascertain a lower limit for half-life determination. Here, 30 s count durations were used instead of 5 min, and three measurements were spread evenly across a 20 min acquisition window (results not shown). However, with such short count times and acquisition window, a reliable calculation of the radionuclide half-life could not be obtained. More investigation will be required to

determine a suitable compromise between count times, acquisition window, and accuracy of half-life.

Analysis of [^{18}F]FDG radiotracer

Having established the linearity of the SiPM signal to activity and the ability to determine half-life, the platform was tested using a sample of [^{18}F]FDG, a [^{18}F]fluoride-labelled glucose analogue that is used in oncology, cardiology and neurology.[7] A single dose of [^{18}F]FDG (487 MBq in 2.3 mL) was produced using the ABT Biomarker Generator, and 40 µL was added to a polycarbonate chip (4 mm thick). The activity in the chip was measured in a dose calibrator and then placed on the SiPM array.

The SiPM signal was measured for 5 min at several time points as the [^{18}F]FDG sample decayed, and the resultant count rates were compared to the [^{18}F]fluoride taken from the linearity study for 4 mm thick polycarbonate (see Fig. 5a). The results are shown in Fig. 6a, and clearly demonstrate how closely the [^{18}F]FDG count rates match the [^{18}F]fluoride, as would be expected since the radionuclide is the same. Most significantly, the results demonstrate that the SiPM platform, with appropriate calibration, can be used to determine the amount of radioactivity (and thus concentration in MBq mL^{-1}) of an unknown sample of a PET radiotracer that contains the same radionuclide.

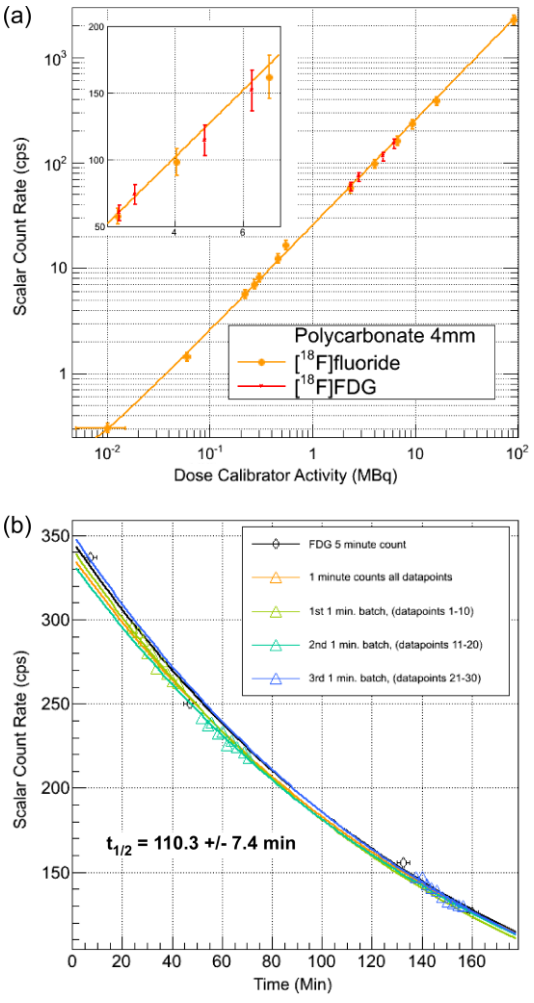

Fig. 6 (a) The fit of SiPM signals for [^{18}F]FDG (red) to the linearity plot of [^{18}F]fluoride (orange) taken from Fig. 5a, demonstrating the potential for the determination of activity levels of radiotracer samples. The substrate was 4 mm thick polycarbonate (PC4). (b) Measurement of [^{18}F]fluoride half-life from a sample of [^{18}F]FDG. The dataset was reanalysed with different parameters to determine the likely limitations of the system.

Furthermore, as with the [^{18}F]fluoride measurements, an exponential could be fitted to the [^{18}F]FDG data to establish the half-life of the sample. A double dataset was taken in this instance. The first was a long time base measurement with the standard 5 min counts taken three times over the course of 160 min (black data points in Fig. 6b). Between these 5 min counts a second dataset was taken in parallel to investigate the limitations of both sample rate and time base. Here, three batches of counts were recorded over 160 min, with each batch consisting of ten 60 s counts taken at approximately 60 s intervals (i.e. ~20 min total per batch). The data points are illustrated in Fig. 6b, with batch 1 (data points 1-10) shown in light green, batch 2 (data points 11-20) in turquoise, and batch 3 (data points 21-30) in blue.

These data were then analysed in two ways. In the first method, both the 5 min count and the 60 s count data points had an exponential curve fitted to extract the half-life in the same manner as for the [^{18}F]fluoride measurements. The 60 s counts were combined into a single dataset and then successively down-sampled, with further fits performed. The result was that down-sampling had a negligible effect on the calculated half-life, even when greatly reducing the number of data points from 30 (three batches of ten readings each) down to 5. However, a reduction in the time base to consider a single 20 min batch produced wildly inaccurate results.

The second data analysis technique was to constrain the fit of the 60 s data points by calibrating with the long time base data and then fitting over a dataset with a time base more acceptable to a final product (approximately 20 min). The fit parameters from the long time base (5 min counts) data were extracted and used to constrain the slope parameter of the exponential fit to the short time base (60 s counts) batches, with the limits of the constraint set to ±1σ, while allowing the constant parameter to be freely varied. Both sets of data are shown in Fig. 6b, with the constrained exponential fits used to determine the half-life. This technique was applied to data with a time base of 20 min and counting times of 60 s and produced a far more accurate result than allowing full degrees of freedom. The half-life calculated by this method was found to be 110.3 ± 7.4 min by limiting the constraint of the exponential fit by 1σ, offering reasonable accuracy for determining the half-life of a [^{18}F]fluoride-labelled radiotracer in a microfluidic channel with a suitable QC time frame of 20 min. However, as discussed in the previous section, further characterisation, optimisation, and the use of a dedicated setup will be needed to achieve the precision required for clinical use, and this will form an essential part of future experiments.

These analytical methods thus demonstrate the suitability of the SiPM setup for satisfying the demands of the *Pharmacopoeia* in terms of the required accuracy and time frame.

Analysis of [^{68}Ga]gallium-citrate radiotracer

Having performed investigations of the SiPM platform using the [^{18}F]fluoride the [^{18}F]fluoride-labelled radiotracer, [^{18}F]FDG, we also wished to determine the technique's suitability to measuring other radioisotopes/radiotracers used in PET medical imaging. [^{68}Ga]gallium is garnering a great deal of interest for use in PET imaging, thanks to its short half-life ($t_{½}$ = 68 min) and decay characteristics,[59-61] and the ability to produce the radionuclide using a compact ^{68}Ge/^{68}Ga generator. In recent years, the labelling of PET tracers with [^{68}Ga]gallium for PET imaging has been achieved in microfluidic devices,[23, 62-65] and so the ability to analyse these radiotracers in a miniaturised platform is highly relevant. Here, we prepared a solution of [^{68}Ga]gallium-citrate, a PET radiotracer used for the imaging of infection, inflammation and tumours,[66-69] as a test model for the SiPM platform.

A solution of the [^{68}Ga]gallium-citrate (40 μL) was introduced into transparent polycarbonate (4 mm, 6 mm, and 8 mm thick), PMMA (4 mm) and B270 glass (6 mm) chips. The results, shown in Fig. 7, demonstrated that the positron-emitting [^{68}Ga]gallium radioisotope could be detected using the SiPM array. Similar trends to the [^{18}F]fluoride results were obtained, with the detection signal increasing linearly with radioactivity, and activity values up to around 8 MBq yielding similar count rates between the two radioisotopes. As before, reducing the thickness of the PC substrate yielded a much greater increase in signal, while signal was also observed in the PMMA and B270 glass substrates. The PMMA showed results that are considered to be unreliable in terms of absolute values due to the problems with the fabrication mentioned previously, but nonetheless showed a linear response in terms of the trend. Tests were also performed using opaque PTFE and (painted) PC substrates, with detection signals once more highlighting the fact that while Cherenkov light may contribute to the detection signal, the main modes of detection occurring appear to be direct interaction between positrons and/or γ rays with the SiPM array.

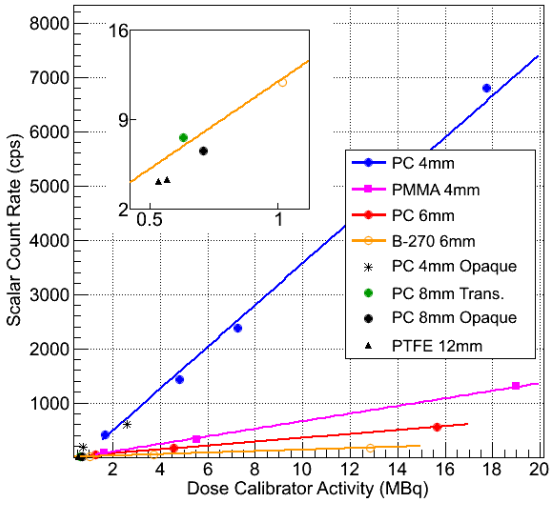

Fig. 7 Activity of the PET radiotracer, [^{68}Ga]gallium-citrate, versus the SiPM count rate for a variety of microfluidic chip substrates and thicknesses. The inset results highlight measurements taken using opaque chips.

The results highlighted that the SiPM detection system was suitable for a variety of radioisotopes and radiotracers, which could include [^{11}C]carbon-based radiopharmaceuticals that are of interest due to their short half-life ($t_{½}$ = 20.4 min)[56] and like-for-like atom replacement in well characterised organic drug molecules to give a negligible radionuclide effect compared to the addition of [^{18}F]fluoride.[1]

Analysis of [^{99m}Tc]pertechnetate radiotracer

While the detection of positron-emitting radioisotopes had been demonstrated, the results had suggested that the SiPM array may have been measuring γ rays directly as one of the sources of signal. In order to study this further, we investigated the measurement of the 140 keV gamma-emitter, [^{99m}Tc]technetium ($t_{½}$ = 6 hours). [^{99m}Tc]technetium is one of the most common clinical radioisotopes used in SPECT imaging radiotracers.[1, 70-72] Thus, in addition to exploring whether the SiPM platform was indeed sensitive to γ rays, a positive result would also show potential for the measurement of SPECT radiotracers as well as PET radiotracers.

[^{99m}Tc]technetium was eluted from a generator as sodium [^{99m}Tc]pertechnetate ($Na^{99m}TcO_4$). This molecule provides a starting material for the radiolabelling of other SPECT radiotracers, but is also used as a radiopharmaceutical itself for imaging of the brain (blood perfusion) and the thyroid (morphology, vascularity, and function).[73] The [^{99m}Tc]pertechnetate solution was diluted in purified water to the required level of activity and pipetted (40 μL) into a 4 mm thick B270 glass chip for counting over 5 min. The chip contained 5.3 MBq of [^{99m}Tc]pertechnetate, which yielded signals of 1.7 – 4.2 cps (502 - 1252 counts over 5 min) depending on the SiPM output channel, easily demonstrating positive detection of the gamma-emitting species above the background levels (0 - 7 counts over 5 min, max. 0.02 cps).

It is worth noting, however, that the count numbers were around 10^3 times lower than similar activities of [^{18}F]fluoride and [^{68}Ga]gallium in the 4 mm thick B270 glass substrates. This is probably due to the difference in mass attenuation coefficients for 140 and 511 keV photons (tabulated at 1.389 x 10^{-1} cm^2 g^{-1} and 8.696 x 10^{-2} cm^2 g^{-1} respectively, in borosilicate glass),[74] whereby the lower energy photons are attenuated to a greater extent and are less likely to hit the SiPM. Nonetheless, the detection of [^{99m}Tc]technetium proved that, even in the absence of positrons and Cherenkov light (which is generated as positrons pass through a material), the SiPM array was sensitive to direct interaction with γ rays, albeit to a much lower extent compared to the effects of positron emission shown in our earlier studies. Scintillation in the glass may also be a possibility, although B270 glass is certainly not renowned for being a scintillator and so any light generated

would be at a very low level. This could be tested in future by repeating the material opacity studies with [^{99m}Tc]technetium.

The ability to detect signals from a [^{99m}Tc]technetium-labelled radiotracer means that the detection setup discussed here, in addition to being suitable for PET radiotracers, also demonstrates potential for the determination of the activity and half-life of gamma-emitting SPECT radiotracers. This greatly broadens the scope of the integrated quality control microfluidic device we are developing to include SPECT as well as PET radiotracers. However, the ability to directly detect γ rays also highlights new chip design considerations for such a QC platform, since an SiPM detector placed on the chip would detect γ rays from any other on-chip location containing gamma-emitters (for SPECT) or positron-emitters (for PET), such as inlet/outlet channels and tubing. This could be quite readily be addressed in future microfluidic devices, though, by employing intelligent channel designs, having extra SiPMs present to allow background correction, or by surrounding the SiPMs in a small amount of shielding such that radioactivity is only detected in the region of interest.

Conclusions

We have investigated the use of low-cost, commercially available SiPMs for the detection of radioactivity within microfluidic channels, towards quality control testing of PET radiotracers. Microfluidic devices fabricated from common substrates were placed directly onto an array of SiPMs, whereupon it was found that the type of chip material had an almost negligible effect, while the thickness of the substrate had a profound influence. We also determined that, despite being light sensors, the bulk of the SiPM signal occurred due to direct interaction of the positrons and γ rays emitted from the radioactive sources. Finally, we demonstrated the application of the SiPM array for the determination of the activity level and half-life of [^{18}F]FDG, as well as detection of the PET radiotracer, [^{68}Ga]gallium-citrate, and the SPECT radiotracer, [^{99m}Tc]pertechnetate. The results provide the groundwork from which more focused radioanalysis systems can be built for a wide range of PET and SPECT tracers, with the findings enabling optimisation of the design of a dedicated microfluidic quality control device. Further studies will involve characterisation of sources of the signal, noise and error that will in turn be used, in addition to other improvements, to optimise the setup for achieving more precise half-life measurements. Evaluation of the spatial resolution and acquisition times that can be achieved with such an optimised SiPM platform will lead to development of the setup towards microfluidic radio-TLC and radio-HPLC analyses, with particular interests being the ability to measure separated plugs of radioactivity in flow.

Acknowledgements

The authors from the University of Sheffield would like to acknowledge the support of LabLogic Systems Ltd., the STFC, and the EPSRC for the funding via the Impact Acceleration Awards. The authors from the University of Hull wish to thank the Daisy Appeal (grant no. DAhul2011) and HEIF (University of Hull) for financial support, and thank Dr Assem Allam and his family for the generous donation to help found the PET Research Centre at the University of Hull and for their continued support. The authors thank Gonçalo S. Clemente for the preparation of [^{18}F]fluoride and [^{68}Ga]gallium-citrate, Hayley A. Bignell for the preparation of [^{99m}Tc]pertechnetate, and Benjamin P. Burke for comments on the manuscript.

References

1. S. L. Pimlott and A. Sutherland, *Chem. Soc. Rev.*, 2011, **40**, 149-162.
2. M. E. Phelps, *Annu. Rev. Nucl. Part. Sci.*, 2002, **52**, 303-338.
3. D. J. Schlyer, *Ann. Acad. Med. Singapore*, 2004, **33**, 146-154.
4. M. M. Khalil, J. L. Tremoleda, T. B. Bayomy and W. Gsell, *Int. J. Mol. Imaging*, 2011, **2011**, 796025.
5. G. Mariani, L. Bruselli, T. Kuwert, E. Kim, A. Flotats, O. Israel, M. Dondi and N. Watanabe, *Eur J Nucl Med Mol Imaging*, 2010, **37**, 1959-1985.
6. K. Hamacher, H. H. Coenen and G. Stocklin, *J. Nucl. Med.*, 1986, **27**, 235-238.
7. B. Beuthien-Baumann, K. Hamacher, F. Oberdorfer and J. Steinbach, *Carbohydr. Res.*, 2000, **327**, 107-118.
8. T. Ido, C. N. Wan, V. Casella, J. S. Fowler, A. P. Wolf, M. Reivich and D. E. Kuhl, *J. Labelled Compd. Radiopharm.*, 1978, **14**, 175-183.
9. P. H. Elsinga, *Nucl. Med. Rev.*, 2012, **15**, C13-C16.
10. P. Y. Keng, M. Esterby and R. M. Van Dam, "Emerging Technologies for Decentralized Production of PET Tracers", in *Positron Emission Tomography - Current Clinical and Research Aspects*, ed. C.-H. Hsieh, InTech, 2012.
11. M.-W. Wang, W.-Y. Lin, K. Liu, M. Masterman-Smith and C. K.-F. Shen, *Mol. Imaging*, 2010, **9**, 175-191.
12. G. Pascali, G. Mazzone, G. Saccomanni, C. Manera and P. A. Salvadori, *Nucl. Med. Biol.*, 2010, **37**, 547-555.
13. G. Pascali, G. Nannavecchia, S. Pitzianti and P. A. Salvadori, *Nucl. Med. Biol.*, 2011, **38**, 637-644.
14. V. Arima, G. Pascali, O. Lade, H. R. Kretschmer, I. Bernsdorf, V. Hammond, P. Watts, F. De Leonardis, M. D. Tarn, N. Pamme, B. Z. Cvetkovic, P. S. Dittrich, N. Vasovic, R. Duane, A. Jaksic, A. Zacheo, A. Zizzari, L. Marra, E. Perrone, P. A. Salvadori and R. Rinaldi, *Lab Chip*, 2013, **13**, 2328-2336.
15. V. Awasthi, J. Watson, H. Gali, G. Matlock, A. McFarland, J. Bailey and A. Anzellotti, *Appl. Radiat. Isot.*, 2014, **89**, 167-175.
16. M. D. Tarn and N. Pamme, "Microfluidics", in *Elsevier Reference Module in Chemistry, Molecular Sciences and Chemical Engineering*, ed. J. Reedijk, Elsevier, Waltham, MA, 2013.
17. S. Y. Lu and V. W. Pike, "Micro-reactors for PET tracer labeling", in *PET Chemistry - The Driving Force in Molecular Imaging*, eds. P. A. Schubiger, L. Lehmann and M. Friebe, 2007, vol. 62, pp. 271-287.
18. G. Pascali, P. Watts and P. A. Salvadori, *Nucl. Med. Biol.*, 2013, **40**, 776-787.
19. C. Rensch, A. Jackson, S. Lindner, R. Salvamoser, V. Samper, S. Riese, P. Bartenstein, C. Wängler and B. Wängler, *Molecules*, 2013, **18**, 7930-7956.

20. P. Watts, G. Pascali and P. A. Salvadori, *J. Flow Chem.*, 2012, **2**, 37-42.
21. P. W. Miller, *J. Chem. Technol. Biotechnol.*, 2009, **84**, 309-315.
22. K. Liu, M.-W. Wang, W.-Y. Lin, D. L. Phung, M. D. Girgis, A. M. Wu, J. S. Tomlinson and C. K.-F. Shen, *Curr. Org. Synth.*, 2011, **8**, 473-487.
23. Y. Liu, M. Tian and H. Zhang, *BioMed Res. Int.*, 2013, **2013**, 839683.
24. J. C. Hung, *J. Nucl. Med.*, 2002, **43**, 1495-1506.
25. S. Yu, *Biomed. Imaging Interv. J.*, 2006, **2**, e57.
26. S. J. Archibald, N. Pamme, N. J. Brown and M. D. Tarn, *J. Nucl. Med.*, 2015, **56**, *suppl. 3*, 167.
27. M. D. Tarn, N. J. Brown, N. Pamme and S. J. Archibald, *J. Labelled Compd. Radiopharm.*, 2015, **58**, S20.
28. P. A. Čerenkov, *Physical Review*, 1937, **52**, 378-379.
29. J. B. Birks, *The Theory and Practice of Scintillation Counting*, Pergamon Press, London, 1964.
30. M. Lavén, S. Wallenborg, I. Velikyan, S. Bergström, M. Djodjic, J. Ljung, O. Berglund, N. Edenwall, K. E. Markides and B. Långström, *Anal. Chem.*, 2004, **76**, 7102-7108.
31. M. Laven, I. Velikyan, M. Djodjic, J. Ljung, O. Berglund, K. Markides, B. Langstrom and S. Wallenborg, *Lab Chip*, 2005, **5**, 756-763.
32. S. Sadeghi, V. Liang, S. Cheung, S. Woo, C. Wu, J. Ly, Y. Deng, M. Eddings and R. M. van Dam, *Appl. Radiat. Isot.*, 2013, **75**, 85-94.
33. J. S. Cho, N. T. Vu, Y. H. Chung, Z. T. Yu, R. W. Silverman, R. Taschereau, H. R. Tseng and A. F. Chatziioannou, *2006 IEEE Nuclear Science Symposium Conference Record*, San Diego, CA, 2006.
34. J. S. Cho, N. T. Vu, Z. T. F. Yu, R. W. Silverman, R. Taschereau, T. Hsian-Rong and A. F. Chatziioannou, *2007 IEEE Nuclear Science Symposium Conference Record*, Honolulu, HI, 2007.
35. S. Türkcan, J. Nguyen, M. Vilalta, B. Shen, F. T. Chin, G. Pratx and P. Abbyad, *Anal. Chem.*, 2015, **87**, 6667-6673.
36. J. S. Cho, R. Taschereau, S. Olma, K. Liu, Y.-C. Chen, C. K. F. Shen, R. M. van Dam and A. F. Chatziioannou, *Phys. Med. Biol.*, 2009, **54**, 6757-6771.
37. A. A. Dooraghi, P. Y. Keng, S. Chen, M. R. Javed, C.-J. C. J. Kim, A. F. Chatziioannou and R. M. van Dam, *Analyst*, 2013, **138**, 5654-5664.
38. S. Chen, M. R. Javed, H.-K. Kim, J. Lei, M. Lazari, G. J. Shah, R. M. van Dam, P.-Y. Keng and C.-J. C. J. Kim, *Lab Chip*, 2014, **14**, 902-910.
39. L. Convert, F. Girard-Baril, A. Renaudin, E. Grondin, A. Jaouad, V. Aimez, P. Charette and R. Lecomte, *Nucl. Instr. Meth. Phys. Res. A*, 2011, **652**, 735-738.
40. L. Convert, F. G. Baril, V. Boisselle, J.-F. Pratte, R. Fontaine, R. Lecomte, P. G. Charette and V. Aimez, *Lab Chip*, 2012, **12**, 4683-4692.
41. L. Convert, G. Morin-Brassard, J. Cadorette, D. Rouleau, E. Croteau, M. Archambault, R. Fontaine and R. Lecomte, *IEEE Trans. Nucl. Sci.*, 2007, **54**, 173-180.
42. C. Fang, Y. Wang, N. T. Vu, W.-Y. Lin, Y.-T. Hsieh, L. Rubbi, M. E. Phelps, M. Muschen, Y.-M. Kim, A. F. Chatziioannou, H.-R. Tseng and T. G. Graeber, *Cancer Res.*, 2010, **70**, 8299.
43. N. T. Vu, Z. T. F. Yu, B. Comin-Anduix, J. N. Søndergaard, R. W. Silverman, C. Y. N. Chang, A. Ribas, H.-R. Tseng and A. F. Chatziioannou, *J. Nucl. Med.*, 2011, **52**, 815-821.
44. A. A. Dooraghi, N. T. Vu, R. W. Silverman, R. Farrell, K. S. Shah, J. Wang, J. R. Heath and A. F. Chatziioannou, *Phys. Med. Biol.*, 2013, **58**, 3739.
45. J. Wang, K. Hwang, D. Braas, A. Dooraghi, D. Nathanson, D. O. Campbell, Y. Gu, T. Sandberg, P. Mischel, C. Radu, A. F. Chatziioannou, M. E. Phelps, H. Christofk and J. R. Heath, *J. Nucl. Med.*, 2013, **54**, 1820-1824.
46. A. Mapelli, B. Gorini, M. Haguenauer, S. Jiguet, G. L. Miotto, W. Vandelli, N. V. Triviño and P. Renaud, *Sens. Actuator A*, 2010, **162**, 272-275.
47. P. Maoddi, A. Mapelli, P. Bagiacchi, B. Gorini, M. Haguenauer, G. L. Miotto, R. M. Garcia, F. S. Tehrani, S. Veneziano and P. Renaud, *J. Instrum.*, 2014, **9**, C01019.
48. SensL webpage, *www.sensl.com*, accessed August 2015.
49. *Technical Note: Introduction to the SPM,* SensL, Ireland.
50. A. Anzellotti, J. Bailey, D. Ferguson, A. McFarland, P. Bochev, G. Andreev, V. Awasthi and C. Brown-Proctor, *J Radioanal Nucl Chem*, 2015, **305**, 387-401.
51. A. I. Anzellotti, A. R. McFarland, D. Ferguson and K. F. Olson, *Curr. Org. Chem.*, 2013, **17**, 2153-2158.
52. B. P. Burke, N. Baghdadi, G. S. Clemente, N. Camus, A. Guillou, A. E. Kownacka, J. Domarkas, Z. Halime, R. Tripier and S. J. Archibald, *Farad. Discuss.*, 2014, **175**, 59-71.
53. D. J. Guckenberger, T. E. de Groot, A. M. D. Wan, D. J. Beebe and E. W. K. Young, *Lab Chip*, 2015, **15**, 2364-2378.
54. R. Brun and F. Rademakers, *Nucl. Instr. Meth. Phys. Res. A*, 1997, **389**, 81-86.
55. S. Agostinelli, J. Allison, K. Amako, J. Apostolakis, H. Araujo, P. Arce et al., *Nucl. Instr. Meth. Phys. Res. A*, 2003, **506**, 250-303.
56. Decay Data Evaluation Project (DDEP), Table of Radionuclides, Laboratoire National Henri Becquerel, *http://www.nucleide.org/DDEP_WG/DDEPdata.htm*, accessed August 2015.
57. *British Pharmacopoeia 2012*, TSO, Norwich, 2012.
58. *Chemistry, Manufacturing, and Controls (CMC)*, Silver Spring, 2011.
59. B. P. Burke, G. S. Clemente and S. J. Archibald, *J. Labelled Compd. Radiopharm.*, 2014, **57**, 239-243.
60. S. R. Banerjee and M. G. Pomper, *Appl. Radiat. Isot.*, 2013, **76**, 2-13.
61. T. J. Wadas, E. H. Wong, G. R. Weisman and C. J. Anderson, *Chem. Rev.*, 2010, **110**, 2858-2902.
62. T. D. Wheeler, D. X. Zeng, A. V. Desai, B. Onal, D. E. Reichert and P. J. A. Kenis, *Lab Chip*, 2010, **10**, 3387-3396.
63. D. Zeng, A. V. Desai, D. Ranganathan, T. D. Wheeler, P. J. A. Kenis and D. E. Reichert, *Nucl. Med. Biol.*, 2013, **40**, 42-51.
64. P. He, H. Bignell, M. Tarn, G. Clemente, B. Burke, N. Esfahani, N. Pamme, N. Brown and S. J. Archibald, *Abstr. Pap. Am. Chem. Soc.*, 2015, **250**, FLUO-27.
65. S. J. Archibald and R. Tripier, *Dalton Trans.*, 2015, **44**, 4789-4790.
66. V. Kumar and D. Boddeti, in *Theranostics, Gallium-68, and* V. Kumar and D. Boddeti, "^{68}Ga-Radiopharmaceuticals for PET Imaging of Infection and Inflammation", in *Theranostics, Gallium-68, and Other Radionuclides*, eds. R. P. Baum and F. Rösch, Springer Berlin Heidelberg, 2013, vol. 194, pp. 189-219.
67. A. Rizzello, D. Di Pierro, F. Lodi, S. Trespidi, G. Cicoria, D. Pancaldi, C. Nanni, M. Marengo, M. C. Marzola, A. Al-Nahhas, D. Rubello and S. Boschi, *Nucl. Med. Commun.*, 2009, **30**, 542-545.

68. V. Kumar, D. K. Boddeti, S. G. Evans and S. Angelides, *Curr. Radiopharm.*, 2012, **5**, 71-75.
69. B. P. Burke, N. Baghdadi, A. E. Kownacka, S. Nigam, G. S. Clemente, M. M. Al-Yassiry, J. Domarkas, M. Lorch, M. Pickles, P. Gibbs, R. Tripier, C. Cawthorne and S. J. Archibald, *Nanoscale*, 2015, **7**, 14889-14896.
70. P. D. Benny and A. L. Moore, *Curr. Org. Synth.*, 2011, **8**, 566-583.
71. M. D. Bartholoma, A. S. Louie, J. F. Valliant and J. Zubieta, *Chem. Rev.*, 2010, **110**, 2903-2920.
72. S. Adak, R. Bhalla, K. K. V. Raj, S. Mandal, R. Pickett and S. K. Luthra, *Radiochim. Acta*, 2012, **100**, 95-107.
73. K. Schwochau, *Technetium: Chemistry and Radiopharmaceutical Applications*, Wiley-VCH, Weinheim, 2000, pp. 387-415.
74. J. H. Hubbell and S. M. Seltzer, *Tables of X-Ray Mass Attenuation Coefficients and Mass Energy-Absorption Coefficients* (version 1.4), 2004. [Online] Available: http://physics.nist.gov/xaamdi [2016, January 22]. National Institute of Standards and Technology, Gaithersburg, MD.